Radar Data Product Superresolution under Parameter Variation

Sergey A. Stankevich, Iryna O. Piestova, Artur R. Lysenko

***Abstract*—** Previously, a model for the spatial resolution enhancement of satellite dual-polarization synthetic aperture radar data with physical constraints was proposed, which was to convert different polarizations backscattering into a single type of physical quantities. However, since the integral equation model depends on the roughness of the reflecting surface, a refined model for resolution enhancement with physical constraints is proposed. In which, first, it is necessary to divide the entire scene into roughness classes by unsupervised land cover classification. Then, an iterative calculation of the land surface dielectric permittivity is performed within each of the land cover classes for two polarizations separately to provide the obtained values as close as possible. The granularity/correlation radius is used as an optimization control parameter. Next, a table of the land cover classes characteristics is formed, which is used to calculate the distributions of the dielectric permittivity for two polarizations radar backscattering. Last, the superresolution of the obtained pair of subpixel-shifted images is carried out using any of the known methods.

***Keywords*—**radar remote sensing, land surface statistics, roughness, dielectric permittivity, superresolution.

I. Introduction

The optical satellite data have a great impact on object detection and mapping, but radar data extend remote sensing techniques to all-weather use [1]. The spatial resolution of radar images and their derived data products is very important in radar remote sensing applications. However, the lack of spatial resolution remains a serious problem of radar remote sensing [2].

There are many superresolution methods, which are subdivided by the principle of operation into hardware-based, band-translation and multi-frame fusion. Some super-resolution approaches require several subpixel-shifted images to build an enhanced image [3].

We have previously proposed a physically constrained model for dual-polarization radar data superresolution using the land surface dielectric permittivity data distribution as input [4]. The problem is the model adjusting with the land surface roughness statistical characteristics – both granularity and correlation radius – that can vary for different land cover types. Now we propose the following technique that is based on the need to divide the entire scene into land surface roughness classes using an unsupervised classification of radar data.

II. Materials

The dual-polarization synthetic aperture radar (SAR) image of the Sentinel-1 satellite single-look complex (SLC) data product for 09/17/2019 on the territory of the Kharkov city and the close vicinity area was used in this study. Images were uploaded from the Copernicus Sentinel Data Hub System – Ukraine (http://sentinel.spacecenter.gov.ua). Preliminary processing of images is carried out, which consists of radiometric and geometric correction. Further, a land surface classification is required to subdivide the whole image into classes that reflect differences in the roughness of land surface (Fig. 1). To improve the classification accuracy,

S. A. Stankevich, Scientific Centre for Aerospace Research of the Earth, Institute of Geological Science, National Academy of Sciences of Ukraine, Kiev, Ukraine (e-mail: st@casre.kiev.ua).
I. O. Piestova, Scientific Centre for Aerospace Research of the Earth, Institute of Geological Science, National Academy of Sciences of Ukraine, Kiev, Ukraine (e-mail: pestovai@ukr.net).
A. R. Lysenko, Scientific Centre for Aerospace Research of the Earth, Institute of Geological Science, National Academy of Sciences of Ukraine, Kiev, Ukraine (e-mail: artur.r.lysenko@gmail.com).

additional radar-derived data are used [5, 6], such as polarization ratios, polarization coherence distributions, GLCM statistics, etc. Five classes of the land surface were obtained.

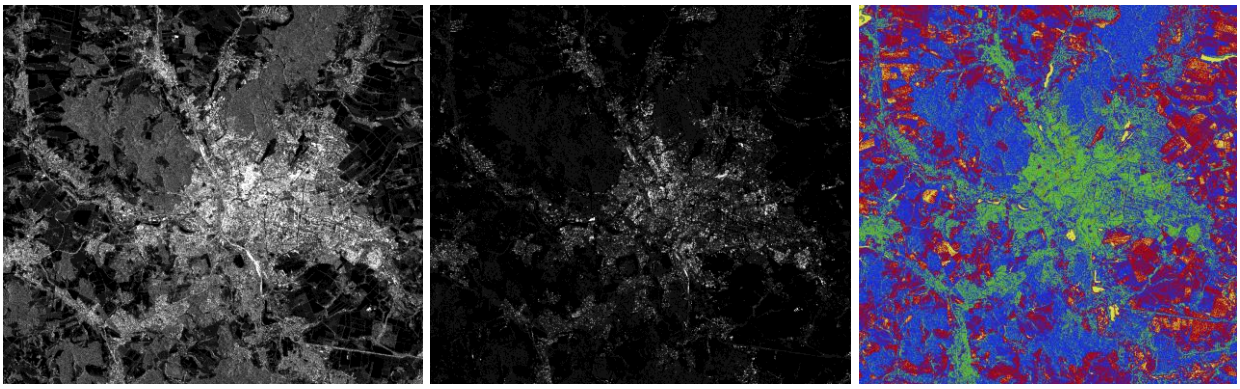

a *b* *c*

Fig. 1 Sentinel-1 satellite SAR data: *a* – σ^0 backscattering value by horizontal (*a*) and vertical (*b*) polarizations and land surface roughness classification (*c*)

Classification map of study area Fig. 1*c* includes land surface roughness classes, which correspond the different types of land cover, such as the tree and grass vegetation, open soil, single-story and high-rise urban development and so on. This classification will be required further for the radar backscattering conversion into the physical characteristic of the land surface.

III. METHOD

The main idea of the applied method is to bring the radar images backscattering values of different polarizations into a unified physical quantity, namely the dielectric permittivity. A well-known Integral Equation Model (IEM) can be used for this purpose [7].

To convert backscattering values sigma nought σ^0 into dielectric permittivity ε we need to know two parameters – the standard deviation s of rough land surface irregularities and the correlation radius l. In the case of two polarizations, the IEM can be written as [8]

$$\alpha = \frac{\sqrt{\sigma^0}}{2k^2 s\cos^2\theta\sqrt{lexp[-kl\sin\theta]^2}} \quad (1)$$

$$\alpha_H = \frac{\varepsilon-1}{(\cos\theta+\sqrt{\varepsilon-\sin^2\theta})} \quad (2)$$

$$\alpha_V = (\varepsilon-1)\frac{(\varepsilon-1)\sin^2\theta+\varepsilon}{(\varepsilon\cos\theta+\sqrt{\varepsilon-\sin^2\theta})^2} \quad (3)$$

where $k = {}^{2\pi}/_{\lambda}$ is the radar wavenumber, λ is the radar wavelength, θ is the radar beam incidence angle, α_H, α_V – are the alpha parameters for the horizontal and the vertical polarizations respectively.

The l parameter value lays in the range 4-10 times of s and can be evaluated for each class independently via numerical computation. In the current case, the l is 4-6 times greater than s. The standard deviation of rough land surface irregularities cannot be much more than one-half of a wavelength due to physical constraints and usually lies in $0.004 \le s \le 0.0125$ m [9].

The s value for each class is established for the point where different polarizations ε values cross. Fig. 2 demonstrates the examples of ε determining.

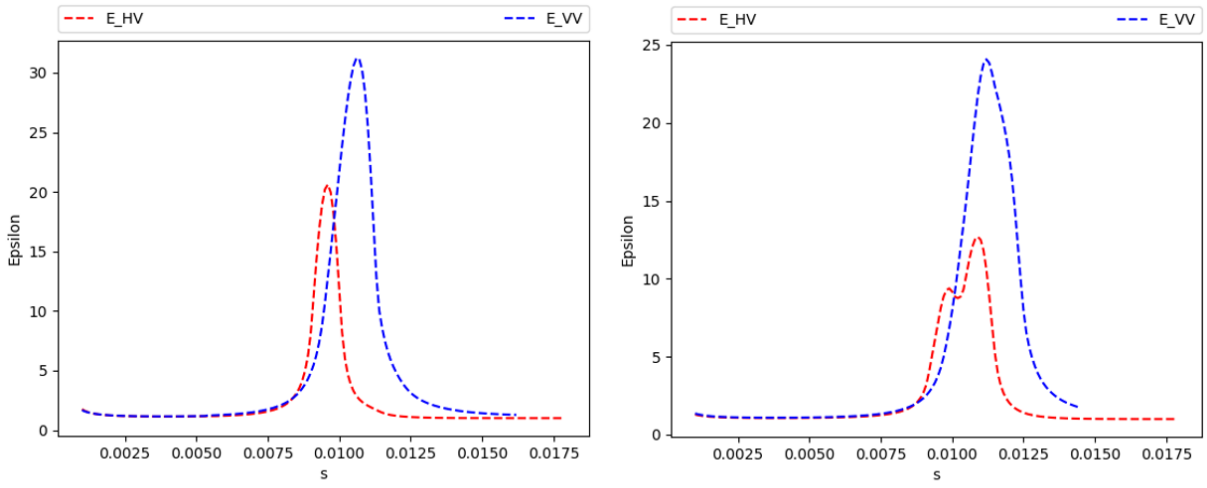

a *b*

Fig. 2 Land surface dielectric permittivity distributions by horizontal (red) and vertical (blue) polarizations: *a* – land surface roughness class 3, *b* – land surface roughness class 1

As shown in Fig. 2, land surface dielectric permittivity does intersect at some points. The points are selected as much far from the epsilon max peaks as possible, due to peaks being an interpolation of ε function model gaps.

According to Fig. 2 plots ε distributions intersect at points $s = 0.008$, $l = 4$ for the class 3 and $s = 0.01$, $l = 4$ for the class 1. Using this approach we have gathered results for each class that are shown in Table 1.

TABLE I
EPSILON CURVES INTERSECTION PARAMETERS

Class number	*s* value	*l* value
1	0.0085	4*s* = 0.034
2	0.0075	5*s* = 0.0375
3	0.0080	4*s* = 0.032
4	0.0058	4*s* = 0.0232
5	0.0050	6*s* = 0.030

Having evaluated all parameters we can now obtain corresponding ε image for both polarizations solving system of equations (1) – (3).

To build the superresolution image we need to estimate the sub-pixel shift between them. It can be done by phase correlation in the frequency domain with special software [10]. After the sub-pixel estimation, we can build an enhanced image using any superresolution technique, e.g. Gaussian regularization [4].

The dataflow diagram in Fig. 3 describes the dual-polarization SAR image processing for land surface dielectric permittivity superresolution.

The difference between the proposed dataflow and the previous one is the more accurate determining the land surface dielectric permittivity taking into account the classification of its roughness.

IV. RESULT

The foregoing method and dataflow applying to radar backscattering data resulted in spatial distributions of unified dielectric permittivity based on the land surface roughness parameters of classes. Obtained distributions are shown in Fig. 4.

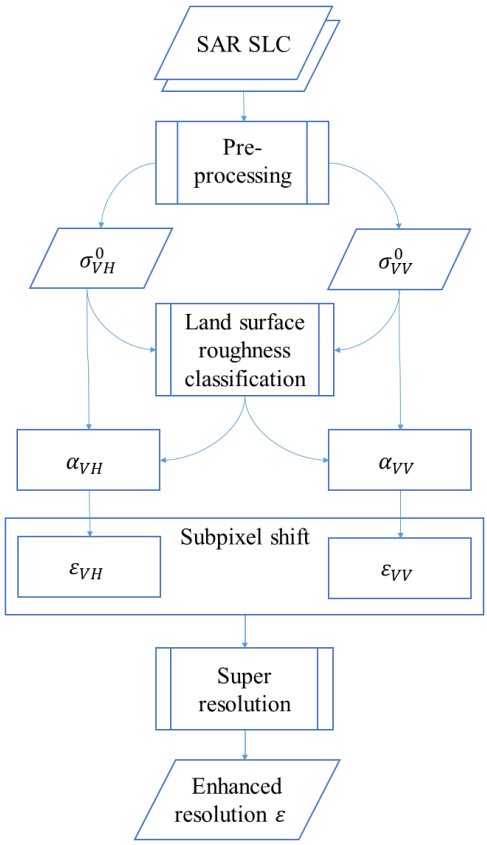

Fig. 3 The dataflow diagram for SAR data product superresolution

The separate cut-through processing of different polarizations radar backscattering combined, firstly, by their synthetic classification of the land surface roughness, and, secondly, by joint processing to obtain an enhanced resolution image of unified dielectric permittivity.

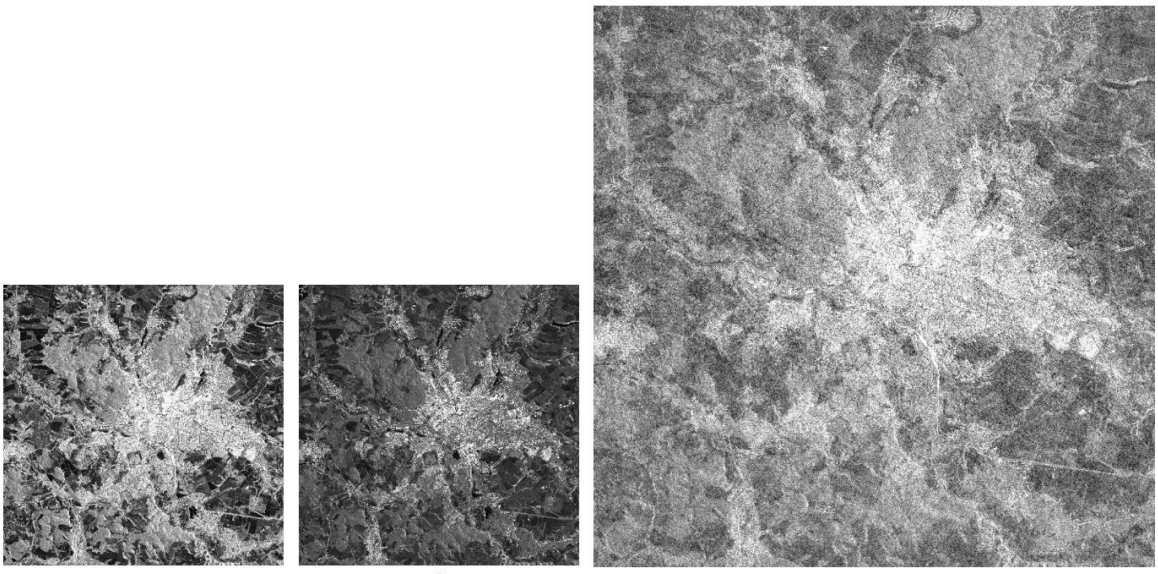

a *b* *c*

Fig. 4 Unified dielectric permittivity maps of study area: *a* – HV polarization derived, *b* – VV polarization derived, *c* – enhanced resolution

A method based on modulation transfer function (MTF) extracted from the digital image was

engaged to quantify the achieved resolution enhancement. This method finds the bidirectional edge spread functions (ESF) within the 4×4 sliding window, corresponding to contrast jumps both horizontally and vertically [11]. Directly measured by images normalized values of the ESF were approximated by integral gaussoid. Averaged ESFs for all three radar data images (Fig. 3) are shown in Fig. 5 plot.

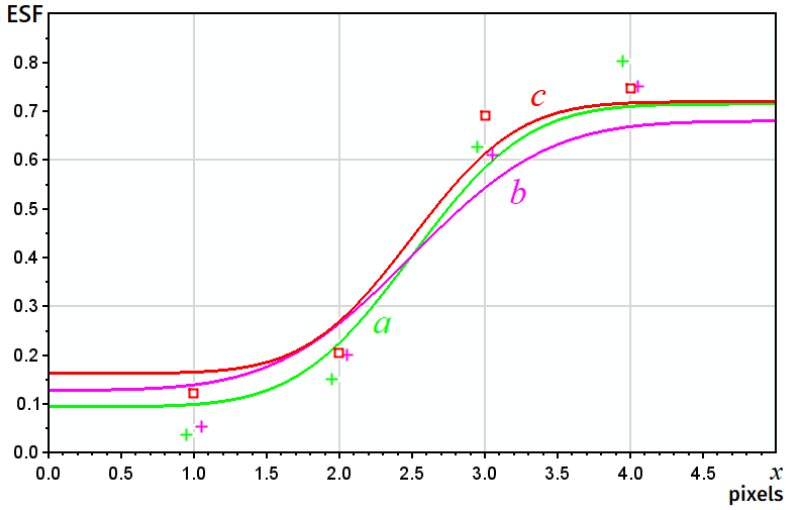

Fig. 5 Measured and approximated ESF of dielectric permittivity images: *a* – HV polarization derived, *b* – VV polarization derived, *c* – enhanced resolution

Gaussian approximation of ESF is determined mainly by two parameters, namely, the steepness of transient response and one's contrast. In turn, spatial resolution is determined only by the first parameter. Gaussian approximation of ESF spatial derivative $h(x)$ can be written as

$$h(x) = \frac{\partial}{\partial x} ESF = \frac{1}{\sigma\sqrt{2\pi}} e^{-\frac{x^2}{2\sigma^2}} \tag{4}$$

where σ is a gaussiod parameter. Hence the MTF $T(\nu)$, ν is a spatial frequency, approximation follows [12]:

$$T(\nu) = e^{-2\pi^2\sigma^2\nu^2} \tag{5}$$

from here the relationship between the spatial resolution r and the σ parameter will be

$$r = \pi\sigma\sqrt{\frac{2}{-\ln T^*}} \tag{6}$$

where T^* = const is the modulation threshold, usually one is given to 0.25 .. 0.5 [13].

Calculated by transient responses Fig. 3 resolution specifications are in Table 2:

TABLE II
ESTIMATED ACTUAL RESOLUTIONS OF RADAR DATA IMAGES FIG. 1

Radar data image	HV polarization derived	VV polarization derived	Enhanced resolution [a]
σ parameter, pixels	0.411	0.476	0.580
resolution r, pixels	1.551	1.797	2.187

Taking into account the half-reducing the formal pixel size in the enhanced resolution image, the actual spatial resolution enhancement is 29.5% for HV polarization derived image, 39.1% for

VV polarization derived image and 34.5% on average. Such value of resolution enhancement for two input images only is a reasonably good result.

V. Conclusion

The described approach to the superresolution of the radar data product seems to be quite efficient. Dual-polarization SAR image test demonstrates enhancement in spatial resolution by 34.5% that makes it a promising method. However, the result is very dependent on classification accuracy. So, the method can be improved by the more accurate acquisition of land surface parameters that affect the restoration of dielectric permittivity. Such improvement can be achieved using multi-polarization radar imagery of higher resolution, as well as by more accurate backscattering models involvement into the computation.

Future work should be aimed to refine the computational algorithms, including algorithms for superresolution, as well as to automate end-to-end processing of radar images within a unified application framework. Another feature of the presented approach, specifically – its physical-driven focus, requires considerable efforts on the ground-based validation the obtained values of the land surface dielectric permittivity.

References

[1] V. Lukin, N. Ponomarenko, A. Kurekin, O. Pogrebnyak. Processing and classification of multichannel remote sensing data. In: I. Batyrshin, G. Sidorov (Eds). Advances in Soft Computing. MICAI 2011. Lecture Notes in Computer Science, vol. 7095. Berlin: Springer, 2011, pp. 487-498. DOI: 10.1007/978-3-642-25330-0_43

[2] J. Singh, M. Datcu. Automated interpretation of very-high resolution SAR images. In: Proceedings of International Geoscience and Remote Sensing Symposium (IGARSS 2012). Munich: IEEE, 2012, pp. 3724-3727. DOI: 10.1109/IGARSS.2012.6350508

[3] V. Agafonov. Super-resolution approach to increasing the resolution of image. In: A. Kravets, M. Shcherbakov, M. Kultsova, T. Iijima (Eds). Knowledge-Based Software Engineering. JCKBSE 2014. Communications in Computer and Information Science, vol. 466. Cham, Springer Nature, 2014, pp. 341-355. DOI: 10.1007/978-3-319-11854-3_29

[4] S. Stankevich, I. Piestova, S. Shklyar, A. Lysenko. Satellite dual-polarization radar imagery superresolution under physical constraints. In: N. Shakhovska, M.O. Medykovskyy (Eds). Advances in Intelligent Systems and Computing IV. CSIT 2019. Advances in Intelligent Systems and Computing, vol. 1080. Cham: Springer Nature, 2020, pp. 439-452. DOI: 10.1007/978-3-030-33695-0_30

[5] H. Zakeri, F. Yamazaki, W. Liu. Texture analysis and land cover classification of Tehran using polarimetric synthetic aperture radar imagery. Applied Sciences, 2017, vol. 7, no. 5, id. 452, 18 p. DOI: 10.3390/app7050452

[6] D. Abudu, N.S. Parvin, G. Andogah. Reviewing the pertinence of Sentinel-1 SAR for urban land use land cover classification. International Journal of Scientific & Engineering Research, 2020, vol. 11, no. 5, pp. 529-535.

[7] A.K. Fung, Z. Li, K.S. Chen. Backscattering from a randomly rough dielectric surface. IEEE Transactions on Geoscience and Remote Sensing, 1992, vol. 30, no. 2, pp. 356-369. DOI: 10.1109/36.134085

[8] M. Choker, N. Baghdadi, M. Zribi, M. El Hajj, S. Paloscia, N.E. Verhoest, H. Lievens, F. Mattia. Evaluation of the Oh, Dubois and IEM backscatter models using a large dataset of SAR data and experimental soil measurements. Water, 2017, vol. 9, no. 1, id. 38., 27 p. DOI: 10.3390/w9010038

[9] M.M. Rahman, M.S. Moran, D.P. Thoma, R. Bryant, E.E. Sano, C.D. Holifield Collins, S. Skirvin, C. Kershner, B.J. Orr. A derivation of roughness correlation length for parameterizing radar backscatter models. International Journal of Remote Sensing, 2007, vol. 28, no. 18, pp. 3995-4012. DOI: 10.1080/01431160601075533

[10] S.A. Stankevich, M.O. Popov, S.V. Shklyar, K.Yu. Sukhanov, A.A. Andreiev, A.R. Lysenko, X. Kun, S. Cao, S. Yupan, S. Boya. Estimation of mutual subpixel shift between satellite images: software implementation. Ukrainian Journal of Remote Sensing, 2020, no.24, pp. 9-14. DOI: 10.36023/ujrs.2020.24.165

[11] S.A. Stankevich. Evaluation of the spatial resolution of digital aerospace image by the bidirectional point spread function parameterization. In: S. Shkarlet, A. Morozov, A. Palagin (Eds). Mathematical Modeling and Simulation of Systems. MODS 2020. Advances in Intelligent Systems and Computing, vol. 1265. Cham: Springer Nature, 2021, pp. 317-327. DOI: 10.1007/978-3-030-58124-4_31

[12] U.V. Gopala Rao, V.K. Jain. Gaussian and exponential approximations of the modulation transfer function. Journal of the Optical Society of America, 1967, vol. 57, no. 9, pp. 1159-1160. DOI: 10.1364/JOSA.57.001159

[13] G.C. Holst. Electro-Optical Imaging System Performance. Bellingham: SPIE Press, 2008, 538 p. ISBN: 9780819474063